

# A Fundamental Study on Inter-Array Cabling Methods Between Two Floating Offshore Wind Turbines in Shallow Waters

Kangho Kim<sup>1</sup>, Chunsik Shim<sup>1</sup>, Min Suk Kim<sup>2</sup>, Daseul Jeong<sup>1,\*</sup>

## ABSTRACT

As the transition to renewable energy accelerates, interest in wind farms is heightening. There is a need to safely and economically transport energy produced from Floating Offshore Wind Turbines (FOWTs) to the shore. Consequently, this study conducted an analysis of inter-array cabling methods between two FOWTs in shallow waters, targeting the southwestern sea of South Korea. This research targeted four shapes of dynamic power cables: free hanging catenary, lazy wave shape, suspended and W-configuration type. To verify the economy of the dynamic power cable, the total lengths were compared, and to check safety, curvature and tension were examined. Insights obtained through this study indicate that among the four shapes of dynamic power cables, the lazy wave shape has substantial advantages in shallow waters.

## KEY WORDS

Inter-array cable; Dynamic power cable; Motion analysis; Excursion.

## INTRODUCTION

As interest in renewable energy grows, there is increasing attention to the production of eco-friendly electricity that can be mass-produced. Among these, the production efficiency of wind energy is relatively high compared to other green energy sources, making the construction of wind farms an essential role in decarbonization. The electricity from a wind farm, which comprises several wind turbines, is transmitted to a substation through power cables after each wind turbine generates it, as shows in Figure 1 (Moon et al., 2014). In this study, we conducted a fundamental study on the methods of transmitting electricity from each wind turbine before it converges at the substation.

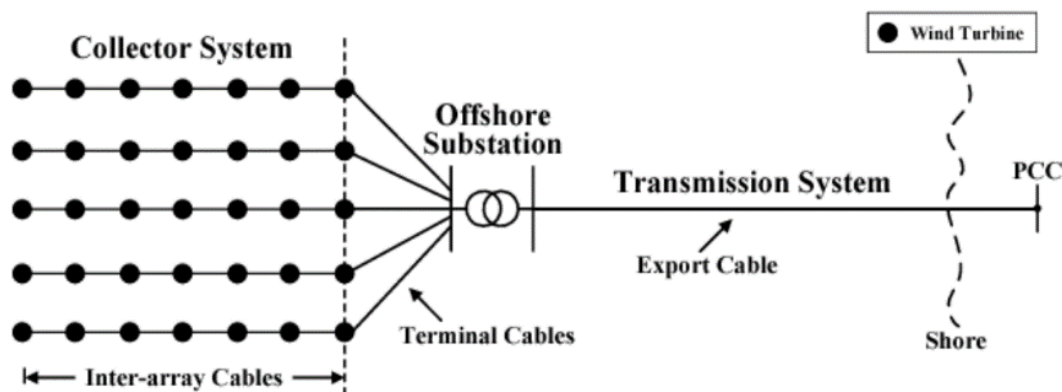


Figure 1: Power transmission system of floating wind farms

<sup>1</sup> Dept. of Naval Architecture and Ocean Engineering, Mokpo National Univ. Republic of Korea. <sup>2</sup> SURF R&D Center, Mokpo National Univ., Republic of Korea.

\* Corresponding Author: dsjeoung@mokpo.ac.kr

Li et al. (2023) developed a dynamic response analysis model for ultra-deepwater cables with double-stepped configurations, focusing on the dynamic responses and robustness to moving boundaries during deep-sea mining operations. The study utilized finite element simulations combined with hydrodynamic models to analyze the cable's behavior under environmental excitations. It concluded that the double-stepped cable design offers improved compliance and effectiveness in buffering responses caused by moving boundaries, contributing to safer and more efficient deep-sea mining operations.

Chen et al. (2021) investigated the structural configurations and dynamic performances of flexible risers with distributed buoyancy modules, using Finite Element Method (FEM) simulations. Their study focused on assessing the influences of buoyancy module positioning and ratio on riser performance, especially under deep-sea mining conditions. The research concluded that the installation positions and buoyancy ratios significantly impact the riser's configuration, tension, and dynamic performance, contributing to the understanding of riser design for safe and effective deep-sea mining operations.

Okpokparoro and Sriramula (2023) conducted a reliability analysis of floating wind turbine dynamic cables under realistic environmental loads. Their research utilized an analytical model to evaluate the fatigue damage and reliability of these cables, considering environmental uncertainties and cable-soil interactions. The study offers significant insights into the structural reliability of dynamic power cables in offshore wind applications, highlighting the importance of considering realistic environmental loads in cable design and reliability assessment.

Poirette et al. (2017) presented a novel optimization methodology for the configuration of inter-array cables in floating offshore wind farms. This study utilizes FEM hydrodynamic simulations in conjunction with a derivative-free Sequential Quadratic Approximation (SQA) optimization algorithm. The research focuses on optimizing the cable layout for minimizing material costs while considering constraints to ensure cable integrity. This approach offers a new perspective on enhancing the efficiency and cost-effectiveness of cable configurations in floating offshore wind farm projects.

Zhao et al. (2021) conducted a study comparing two dynamic power cable configurations for floating offshore wind turbines in shallow water. Their research compared the hydrostatic and hydrodynamic performance of lazy wave and double wave configurations, utilizing a comprehensive numerical simulation approach. The study found that the double wave configuration exhibited superior performance, offering advantages in terms of reduced fatigue damage and better handling of high curvature tension.

Ahmad et al. (2023) explored an optimization methodology for suspended inter-array power cable configurations between two floating offshore wind turbines. Their research focused on the dynamic response of these configurations using a novel setup involving subsea buoys. The study demonstrated the feasibility of the suspended inter-array power cable concept, highlighting those smaller buoys yield more efficient designs and the copper cable configurations result in smaller horizontal excursions compared to aluminum cables.

Rentschler et al. (2019) focused on the design optimization of dynamic inter-array cable systems for floating offshore wind turbines. Utilizing a genetic algorithm, they analyzed cable configurations to improve fatigue life performance under extreme weather conditions. The research highlights the importance of considering dynamic behaviors and offers design recommendations for different water depths, contributing significantly to the development of efficient and reliable floating offshore wind technologies.

Schnepf et al. (2023) conducted a feasibility study on suspended inter-array power cables between two spar-type offshore wind turbines. This research involved exploring various cable configurations and their impact on structural behavior, focusing on buoyancy module placements. The study concluded that certain configurations, particularly those with strategically placed buoyancy modules, can lead to significant improvements in cable performance and cost-effectiveness in offshore wind turbine applications.

Jason Lavis (2021) argued that while shallow water was previously described as having depths of up to 91-121m, today, depths of less than 305m are now considered shallow. Tong (1998) identified the economic depth range for floating offshore wind turbines as typically between 100m and 300m. This study focuses on an area located in the Southwest Sea, with a water depth of 150m, falling well within Tong's suggested economic depth range. This placement offers optimal conditions for installing FOWTs, suggesting a strategic fit for this renewable energy technology in areas previously deemed challenging.

This study builds upon the 12MW FOWT model by SINTEF Norway and, to conduct a fully coupled dynamic analysis, using OrcaFlex to adapt to the ocean data measured from Uido island located in southwestern of Korea. The pivotal research endeavor involves the integration of a dynamic power cable into a 12 MW FOWT, thus considering the mooring system's intricate design. By adhering to the IEC 61400 regulations and realistic maritime conditions found in South Korea's southwestern sea, the study

carries out both Serviceability Limit State (SLS) and Ultimate Limit State (ULS) analyses, ensuring its findings' accuracy and practical relevance. The study focused on four types of power cables: free hanging catenary, lazy wave shape, suspended and W-configuration type.

## METHOD

### Three-column FOWT layout for optimal mooring and cable integration

Figure 2 shows the 12MW substructure model of SINTEF. The model consists of three columns and six pontoons. The main properties of the 12MW FOWT are summarized in Table 1 (SINTEF, 2022).

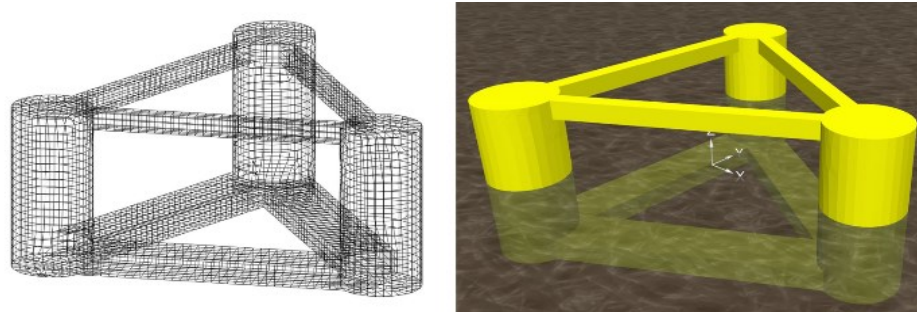


Figure 2: SINTEF 12MW substructure

The coordinate system of the analytical model is designed to align with the global coordinates of the substructure provided by SINTEF, as shown in Figure 3.

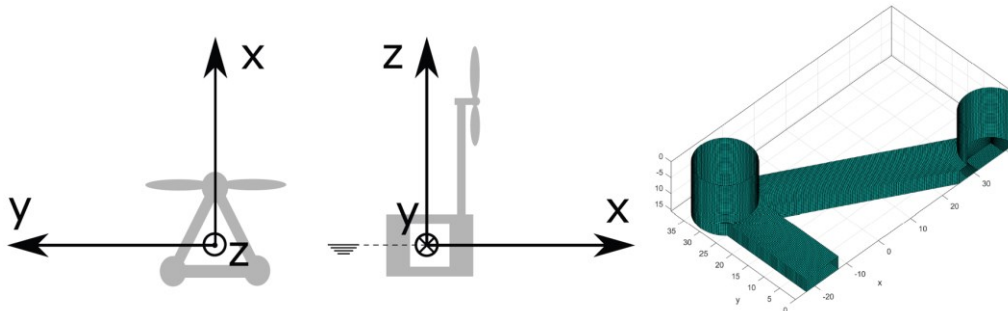


Figure 3: Coordinate system of SINTEF's 12MW offshore wind turbine substructure

To construct a wind farm using a substructure with three columns, the layout presented in Figure 4 by Aker Solutions (2019) is referenced. The model modeled using OrcaFlex is as shown in Figure 5. This configuration is an arrangement of a floater with three columns that shares anchors and ensures there is no interference between power cables and mooring lines. An advantage of using such an arrangement is that it facilitates the expansion for the construction of a wind farm, as illustrated in Figure 6.

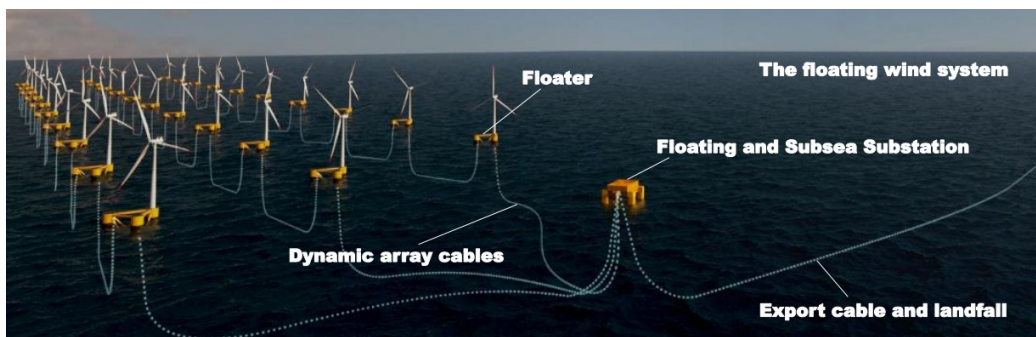
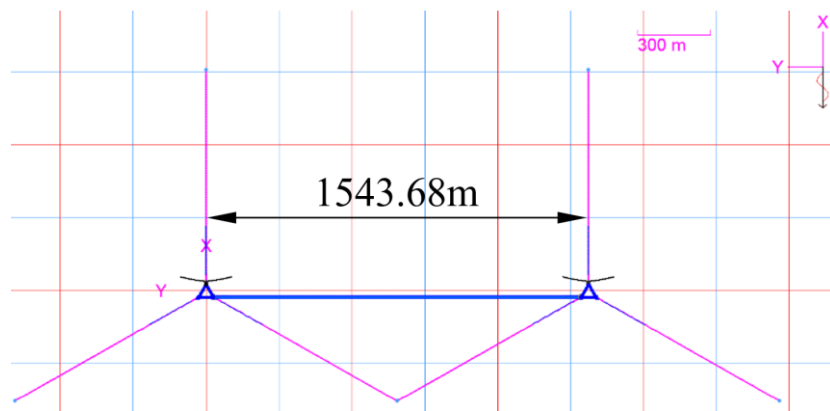


Figure 4: Inter array cable layout

**Table 1: Main properties of the 12MW wind turbine**

Parameter	Properties
Turbine rating	NREL 12MW
Blade length (m)	105.4
Hub diameter (m)	6
Hub Height (m)	131.7
Draft (m)	15.5
Nacelle mass (kg)	600,000
tower mass (kg)	1,161,600
Blade mass (kg)	3 * 63024
Hub mass (kg)	60,000
Total mass (kg)	14,176,000
Cut-in/rated/cut-out wind speed (m/s)	4.0 / 10.6 / 25.0
Cut-in/ rated rotor speed (rpm)	5.5 / 7.8
Generator efficiency (%)	94



**Figure 5: Layout of analysis model (top view)**

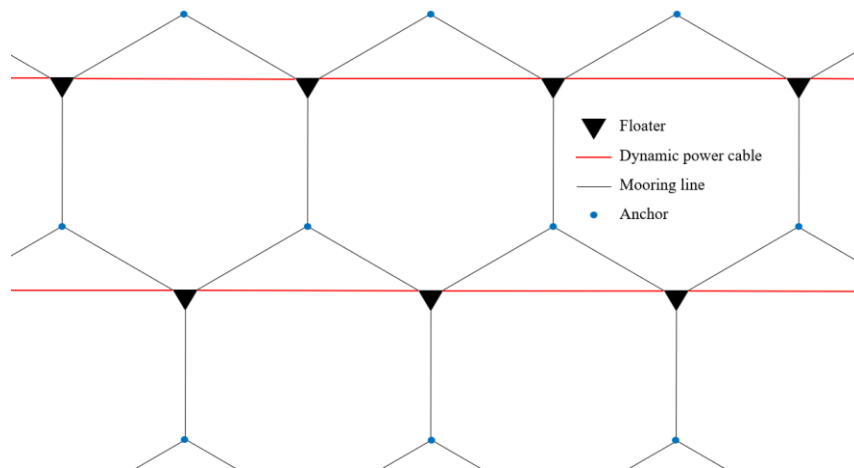


**Figure 6: Expanding the floating substructure with three columns**

The analysis model and the coordinate system used in this process are presented in Figure 7, and the specifications of the designed mooring line are detailed in Table 2. Additionally, Table 3 describes the positions of crucial points such as the fairleads and anchor points for each mooring line in their static state to understand the mooring system.

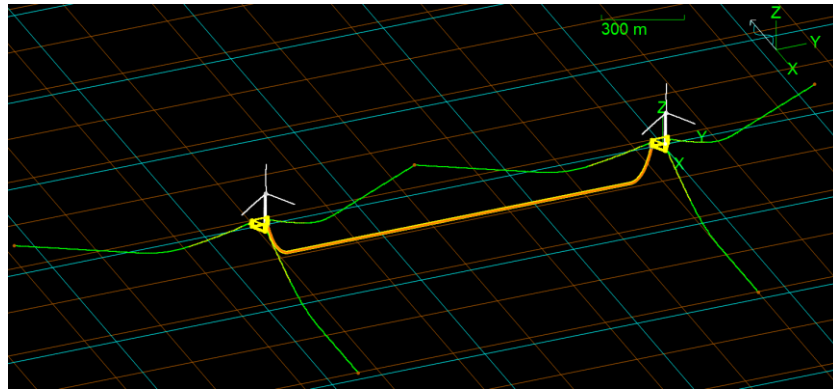


**Figure 7: Overview of the analytical model for offshore wind farm cabling**

**Table 2: Mooring line material and length**

Line type	ML 1	ML 2	ML 3
	Length (m)		
170mm R4 studless platform chain	32.4	32.4	32.4
210mm 6 strand rope	220.0	220.0	220.0
170mm R4 studless ground chain	665.0	660.0	660.0
Total length	917.4	912.4	912.4

**Table 3: Main points of the mooring line position**

		ML1	ML2	ML3	ML1-1	ML2-1	ML3-1
Fairlead point (m)	x	33.0	-31.1	-31.1	33.0	-31.1	-31.1
	y	0.0	-37.0	37.0	-1574.2	-1611.2	-787.1
	z	0.0	0.0	0.0	0.0	0.0	0.0
Anchor point (m)	x	906.1	-454.4	-454.4	906.1	-454.4	-454.4
	y	0.0	-787.1	787.1	-1574.2	-2361.3	-787.1
	z	-150.0	-150.0	-150.0	-150.0	-150.0	-150.0

### Design of the dynamic power cable configurations

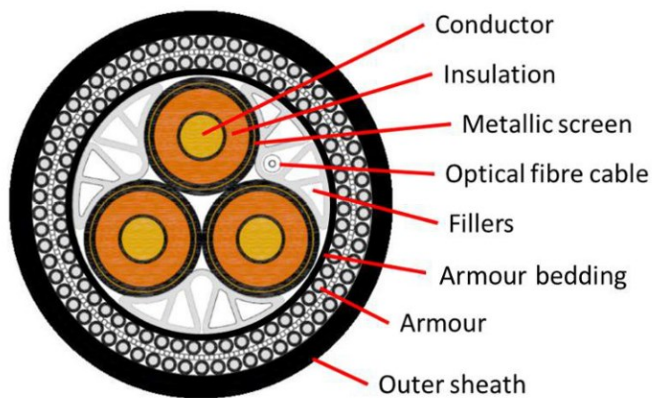


**Figure 8: Typical dynamic cable cross section**

The cross-section of the cable is composed of three conductor cores wrapped in insulation and two steel armour. In addition, it has four helical layers (circular helix type) including a copper shield and an outer sheath to protect the cores. The typical shape of a three-core power cable's cross-section is as shown in Figure 8 (CIGRE, 2022). The capacity of the power cable used in this study is 66kV.

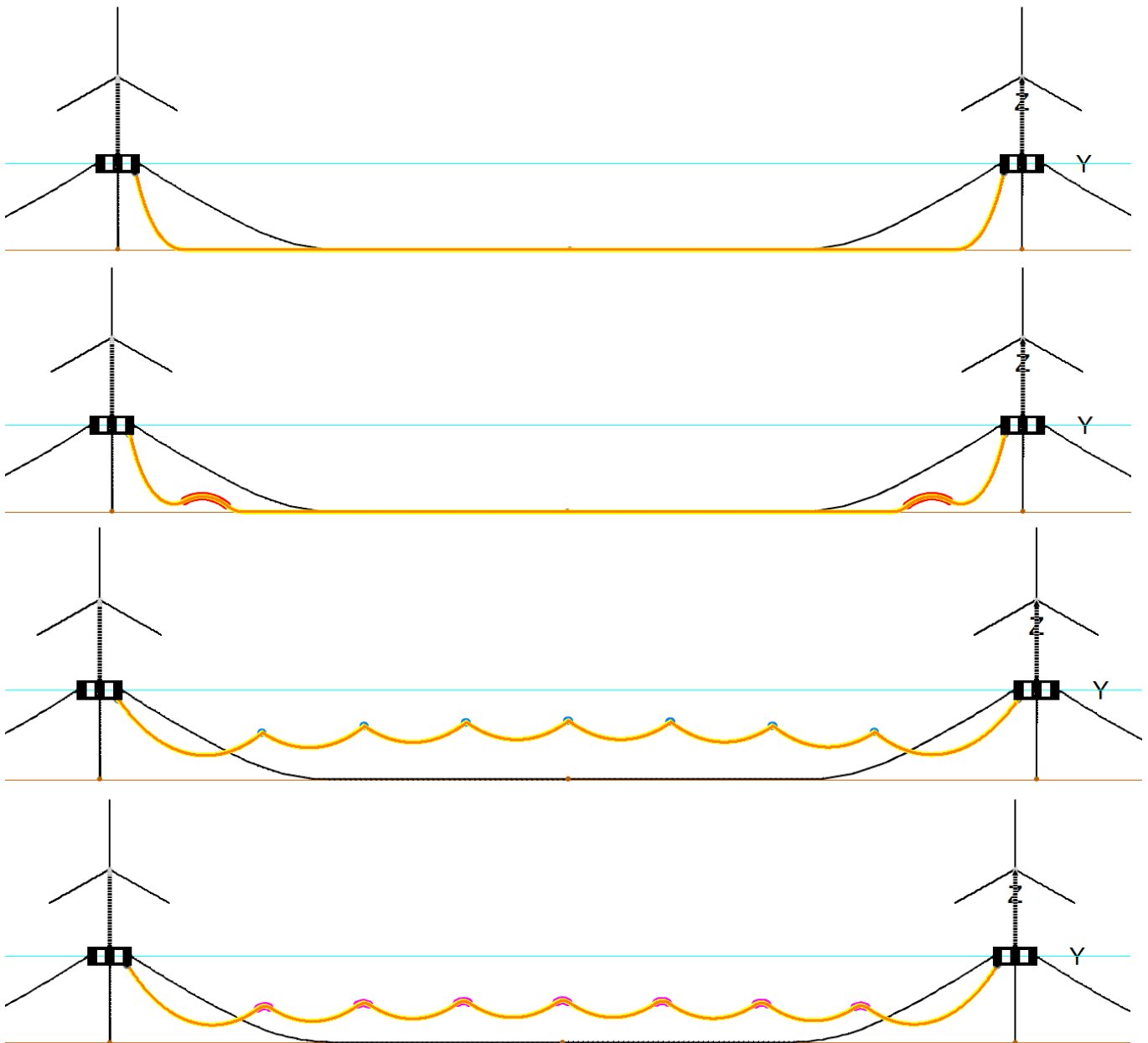


**Figure 9: Cable configurations. From top, (a) free hanging catenary (b) lazy wave shape (c) suspended (d) W-configuration**

Rentschler et al. (2020) conducted a parametric study on the inter-array cable systems of FOWTs. The optimal total cable lengths relative to water depth and buoy placements obtained through the parametric study are referenced for the design of the catenary and lazy wave shapes.

In this study, as shown in Figure 9, simulations are conducted for four types of power cables: (a) free hanging catenary, (b) lazy wave shape, (c) suspended and (d) W-configuration. The depth is set to 150 meters to determine which inter-array cable method is most suitable for shallow water depths.

The total length of the cable is 1681.9 meters, and different types of buoys are used to implement the lazy wave shape, suspended and W-configurations. For the lazy wave shape, relatively small buoys are attached, numbering 62 in total, while

for the suspended configuration, 7 large-capacity buoys are attached. In the W-configuration, 5 buoys are installed in each of the 7 sections, making a total of 35 buoys installed. Detailed specifications of the buoys are as presented in Table 4.

**Table 4: Power cable attachment buoy specification**

	Mass (te)	Volume (m <sup>3</sup> )	Drag coefficient (x)	Drag coefficient (z)	Added mass coefficient (x)	Added mass coefficient (z)
Lazy wave shape buoy	0.069	0.197	1.100	1.100	1.000	1.000
Suspended buoy	2.700	8.615	0.209	1.000	0.459	0.600
W-configuration buoy	0.55	1.72	1.2	1.000	0.459	0.600

Figure 10 displays a detailed comparison between the suspended and W-configuration, zooming in on their structural differences. In the suspended configuration, a single buoy is installed in each section, resulting in a pointed appearance, whereas in the W-configuration, five buoys are installed in a single section, creating a smoother curve. The number and arrangement of buoys have been adjusted to prevent excessive curvature.



**Figure 10: Detailed comparison between suspended and W-configuration**

## Environmental load case

### Wave

To conduct simulations that closely resemble actual conditions at sea, numerous variables such as significant wave height ( $H_s$ ), zero-crossing period ( $T_z$ ), wave direction, tidal speed, and wind speed/direction are identified to establish comprehensive load cases. These variables are not arbitrarily chosen, but meticulously selected and optimized based on an extensive collection and processing of maritime environmental data. The data, harvested from Uido, Sinan, Jeollanam-do, South Korea, spans an entire year in 2021 and comprises 7,853 data points observed at hourly intervals, as shows in Table 5. (KHOA, 2022) waves are implemented using the JONSWAP spectrum with the obtained values for  $T_z$  and  $H_s$ . (Hasselmann, K. et al.)

**Table 5: Wave scatter diagram for Sinan Uido**

$T_z$ (s)	$H_s$ (m)							sum
	0.5	1.5	2.5	3.5	4.5	5.5	6.5	
3.5	834	3	0	0	0	0	0	837
4.5	1,766	121	0	0	0	0	0	1,887
5.5	1,719	600	8	0	0	0	0	2,327
6.5	824	684	101	0	0	0	0	1,609
7.5	370	252	239	9	0	0	0	870
8.5	88	36	40	71	1	0	0	236
9.5	73	24	5	11	4	0	0	87
sum	5,644	1,720	393	91	5	0	0	7,853

## Current

Current is calculated through wind-generated, tidal, and power law methods. (DNV, 2019) The current generated by the wind is determined by multiplying the average wind speed at an altitude of 10m by a coefficient  $k$ , as in Equation 1. The wind speed for the SLS is 18m/s, and for the ULS is 42.5m/s. Precise values of the coefficient  $k$  can be obtained from field measurements or detailed fluid dynamics models, but in this study, an intermediate value of 0.02 was used.

$$v_{c,wind}(0) = kU_{1\text{ hour},10\text{ m}} \text{ where } k = 0.015 \text{ to } 0.03 \quad [1]$$

For the current, the power law method, as detailed in Equation 2, was used to establish varying speeds at the 50m depth and the seabed.  $S_f$  and  $S_b$  denote the current speeds at the surface and seabed, respectively.  $Z_f$  and  $Z_b$  represent the  $Z$  coordinate of the 50m depth and seabed directly below the  $(X, Y)$  coordinates. This study set the power law exponent, denoted as  $p$ , to 7 (Orcina, 2023). The current profile used in this study is as depicted in Figure 11.

$$S = S_b + (S_f - S_b) \left[ \frac{Z - Z_b}{Z_f - Z_b} \right]^{\frac{1}{p}} \quad [2]$$

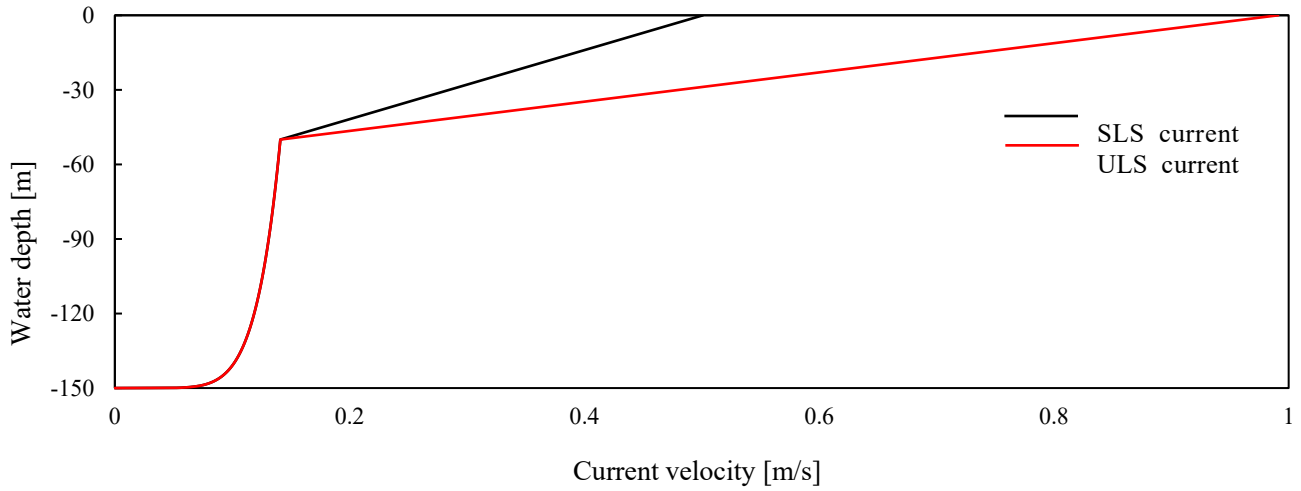


**Figure 11: Current profiles in SLS and ULS**

## Environmental load in a 50-year cycle

The SLS analysis utilizes maximum values, such as significant wave height ( $H_s$  4.5m), zero-crossing period ( $T_z$  9.5s), and wind speed (18m/s). To recognize the potential impact of wave and wind directions on the mooring lines, these elements are set at 180 degrees, 300 degrees, and 60 degrees, resulting in a total of 9 SLS load cases. For the ULS analysis, assumptions are made based on Det Norske Veritas DLC 1.3 (DNV, 2016), with an understanding that the wind and wave directions are aligned.

Table 6 presents the wind speed, derived by examining the standard parameters that classify wind turbine stages in accordance with International Electrotechnical Commission 61400-1 (IEC, 2005). This research utilizes the wind speed recorded at the wind turbine class II stage.  $V_{ref}$  symbolizes the reference wind speed measured over 10 minutes, and A, B, C denote category designation values for high, medium, and low turbulence characteristics, respectively. Additionally,  $I_{ref}$  denotes the anticipated turbulence intensity value at a wind speed of 15m/s.

**Table 6: Basic parameters for wind turbine classes**

Wind turbine class	I	II	III	S
$V_{ref}$ (m/s)	50	42.5	37.5	Values specified by the designer
A $I_{ref}$	0.16			
B $I_{ref}$	0.14			
C $I_{ref}$	0.12			

The extreme wind speeds corresponding to a 50-year return period are determined by referencing the IEC 61400-1 standard, which prescribes the standard wind speeds for three distinct turbine classes. The reference wind speed of 42.5m/s, associated with Class II, is employed in our analysis. For the evaluation of the significant wave height and the zero-crossing period under extreme wind scenarios, the American Petroleum Institute's (API, 2007) 2INT-MET guidelines are consulted. With a considered wind speed of 41.12m/s, the significant wave height is found to be 12.9m, and the zero-crossing period is recorded at 14 seconds. Hence, one ULS load case has been established in this research. The crucial details and visualizations for these load cases, vital for an all-encompassing understanding of the system's behavior, are shown in Table 7 and Figure 12.

**Table 7: Environmental load case**

	Load case	Waves			Wind	
		H <sub>s</sub>	T <sub>z</sub>	Dir.	Speed	Dir
		m	s	degree	m/s	degree
SLS	1	4.5	9.5	180	18.0	180
	2			180		300
	3			180		60
	4			300		180
	5			300		300
	6			300		60
	7			60		180
	8			60		300
	9			60		60
ULS	10	12.9	14.0	180	42.5	180

In this study, ten Environmental load cases are established, and the analysis is conducted targeting the shapes of four power cables. The names for the analysis cases are configured as C-LC1 (Catenary-Load Case1), L-LC1 (Lazy wave-Load Case1), S-LC1 (Suspended-Load Case1) and W-LC1(W-configuration-Load Case1).

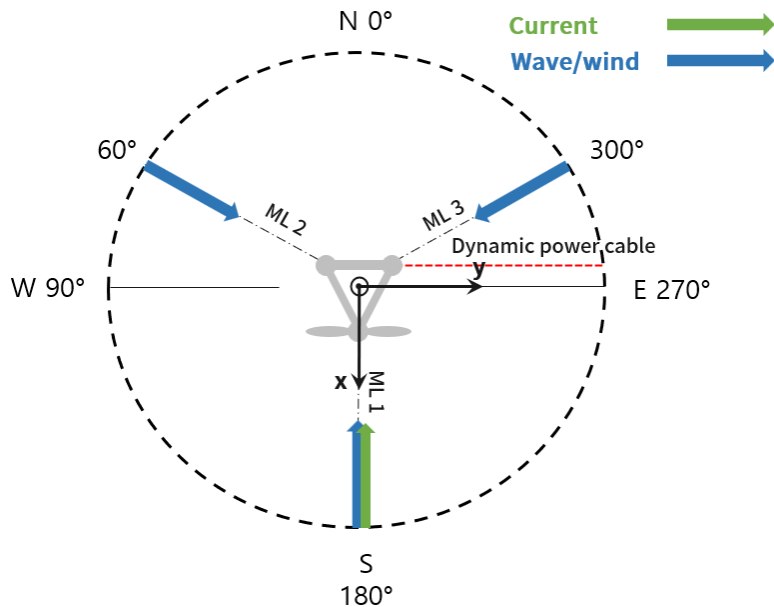


**Figure 12: Load case diagram**

# RESULTS

## Assessing cable configuration performance in LC10

In shallow water depth, a dynamic analysis is conducted using two FOWTs to determine the best method among four cable configurations. The simulation time is 10,800s (3 hours), with a start-up time of 300s, totaling 11,100s of dynamic analysis. Figure 13 shows the maximum elevation state at LC10 after completing the dynamic analysis for each shape. In the case of catenary and lazy wave, the cables lay on the seabed, while in suspended and W-configuration, they float in the middle. The suspended and W-configuration are designed to minimize the impact of wind-generated forces in the maximum elevation state, being set lower than 50 meters in depth.

Figures 14 and 15 illustrate the profiles of maximum effective tension and maximum curvature according to arc length, respectively. The maximum tensions and curvatures for each configuration are summarized in Table 8. The tension of the lazy wave is 19.00% lower than that of the catenary, 25.01% lower compared to the suspended and 26.28% lower compared to the W-configuration. Additionally, the lazy wave demonstrates superior performance in curvature as well, being 30.52% lower than the catenary, 77.42% lower than the suspended and 60.16% lower than the W-configuration. Overall, the performance of the lazy wave shape is confirmed to be superior, and it is advisable to use the lazy wave shape for ensuring long-term fatigue performance of dynamically behaving cables.

The W-configuration is a form designed to prevent the excessive curvature observed in the suspended configuration by installing five buoys in one section. While this significantly reduced the curvature, it was found to offer no substantial advantage in terms of tension. Considering installation and maintenance costs, it becomes evident that the lazy wave shape offers greater benefits.

**Table 8: The rate of increase in tension and curvature for each configuration compared to the lazy wave**

DLC	Maximum tension (kN)	Rate of increase compared to lazy wave (%)	Maximum curvature (m/m)	Rate of increase compared to lazy wave (%)
L-LC10	60.18	0.00	0.1218	0.00
C-LC10	74.29	19.00	0.1753	30.52
S-LC10	80.25	25.01	0.5393	77.42
W-LC10	81.57	26.28	0.3055	60.16

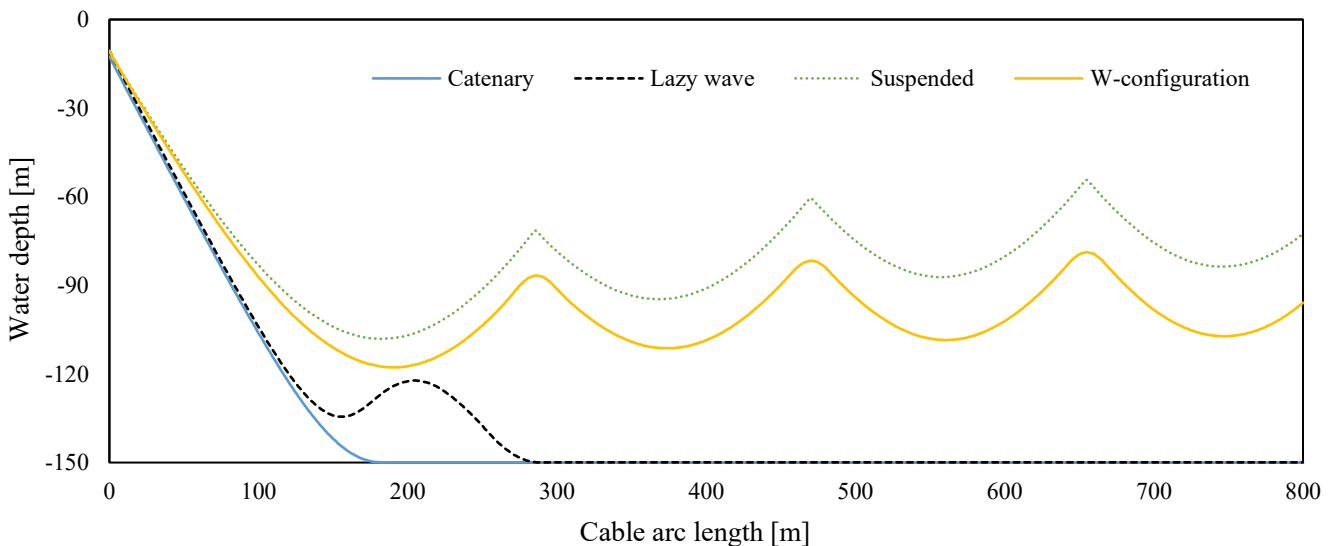


**Figure 13: Cable configuration of maximum elevation state per arc length in LC10**

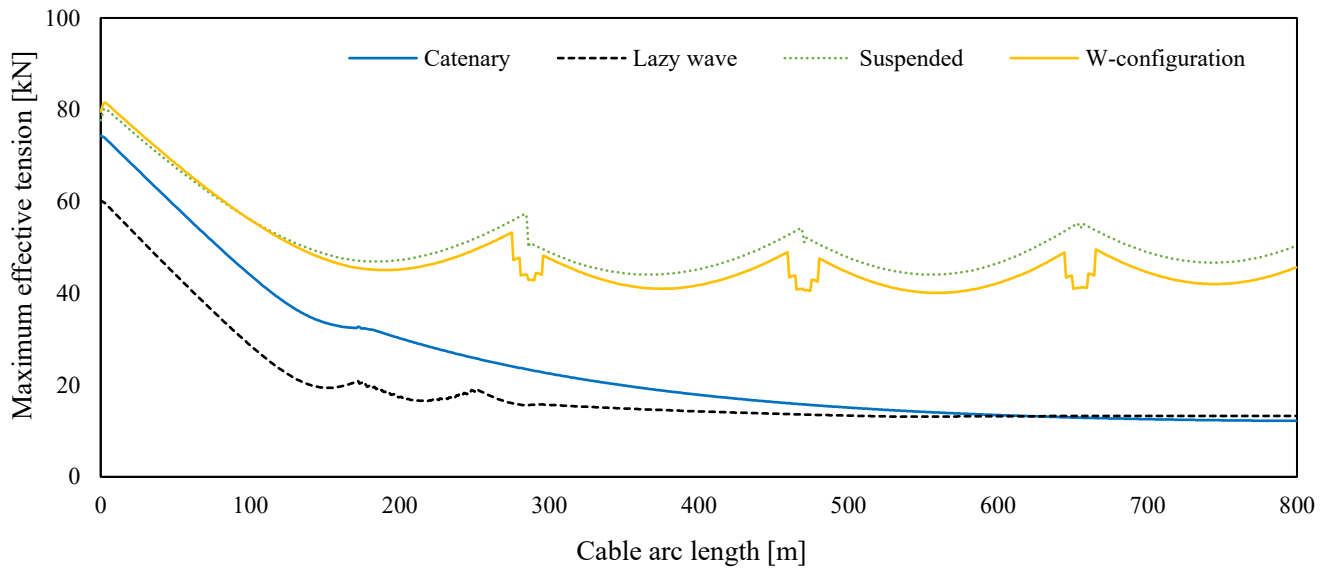


**Figure 14: Maximum effective tension profile for each shape in LC10**

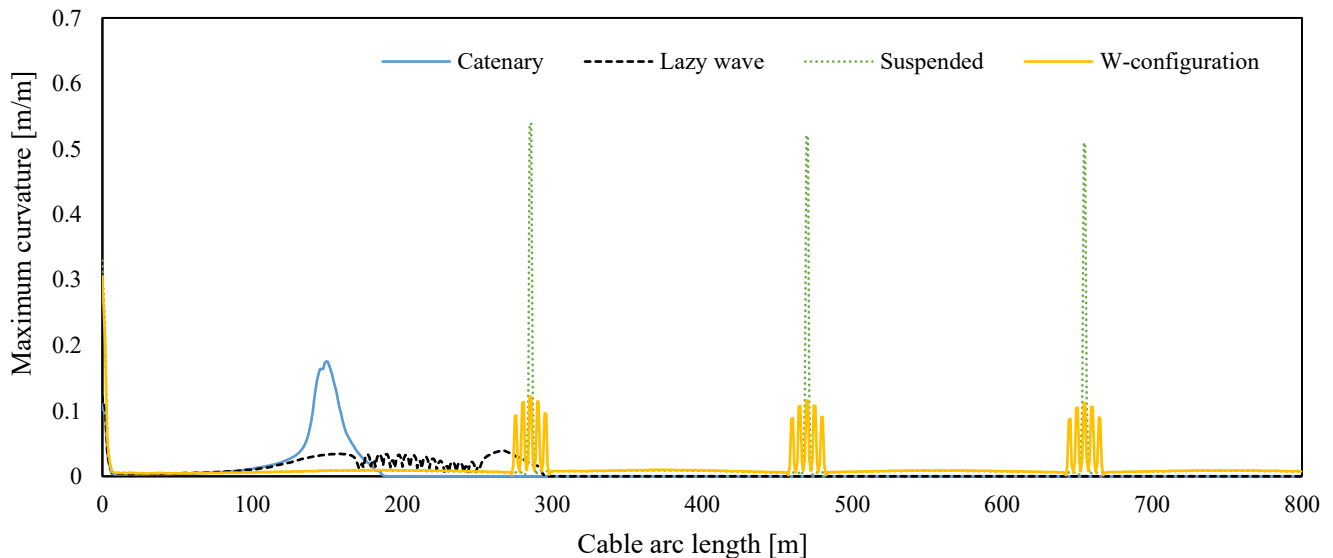


**Figure 15: Maximum curvature profile for each shape in LC10**

### Evaluating all design load cases

Figures 16 and 17 respectively display the values of maximum effective tension and maximum curvature for all load cases. The points of highest tension and curvature in the cable occur at the hang-off connected to the substructure and the touch down point affected by the bottom drag. For the suspended case, since there is no touch down point, the tension and curvature at the buoy nearest to the hang-off are observed, denoted as the ‘1<sup>st</sup> buoy’.

In the case of C-LC10, the curvature and tension at the touch down point show significant differences between the SLS and ULS. This is deemed a characteristic of the free-hanging shape, where movements at the upper part of the power cable induce excessive motion at the lower part. For lazy wave and suspended, the difference between SLS and ULS is not substantial, indicating that the buoys placed in-between prevent excessive transfer of movements from the upper part of the power cable. However, considering the much higher curvature of the suspended compared to the catenary and lazy wave, the lazy wave method appears most suitable for inter-array cabling of power cables in shallow waters.

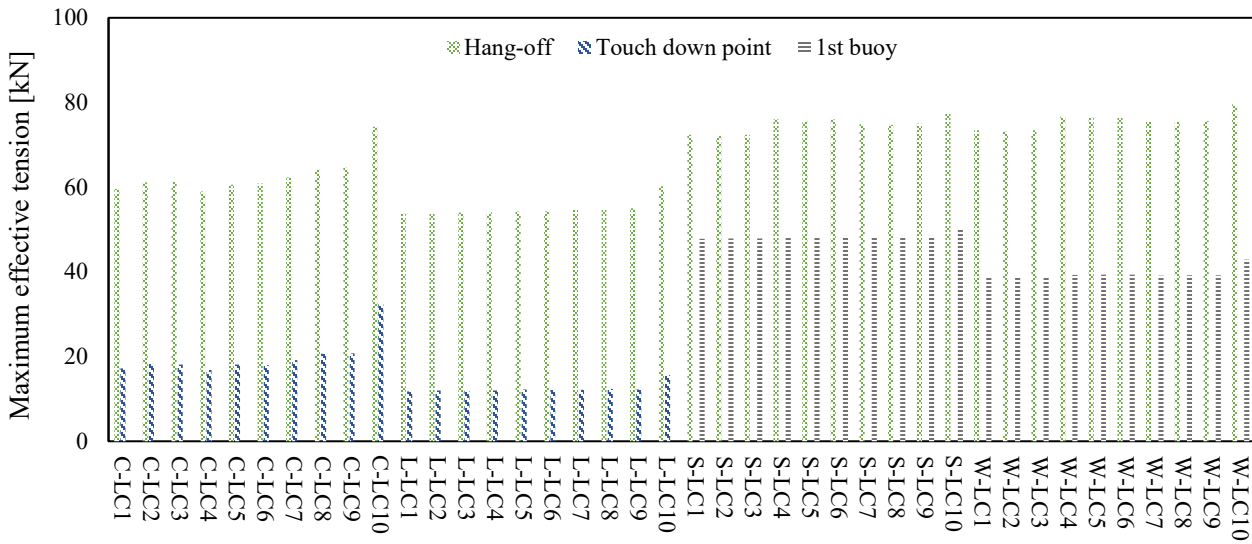


Figure 16: Maximum effective tension for all design load case

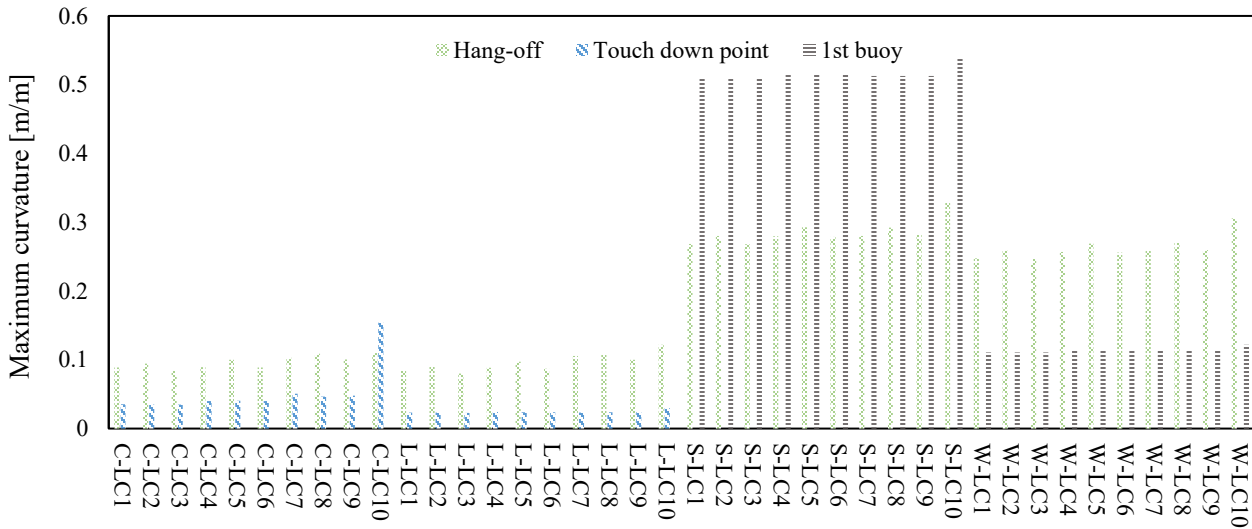


Figure 17: Maximum curvature for all design load case

### Bird caging effect in helical cable

According to the study by Lu et al. (2017), the bird cage buckling phenomenon is likely to occur when the armor wires are subjected to high axial compression that exceeds their critical load, especially if there is damage to the cover sheath and strength tapes, as shows Figure 18.



Figure 18: Bird caging failure mode of tension armor wires

The bird caging phenomenon can occur in steel armor cables that are twisted in one direction and can manifest when excessive compressive loads are applied. Among the four analytical models performed in this study, it was observed that a negative tension occurred at the touch down point of the catenary. As shown in Figure 19, the maximum compressive load was calculated to be 10.71 kN, which is not an absolute large value, but it suggests that caution is needed when designing FOWTs.

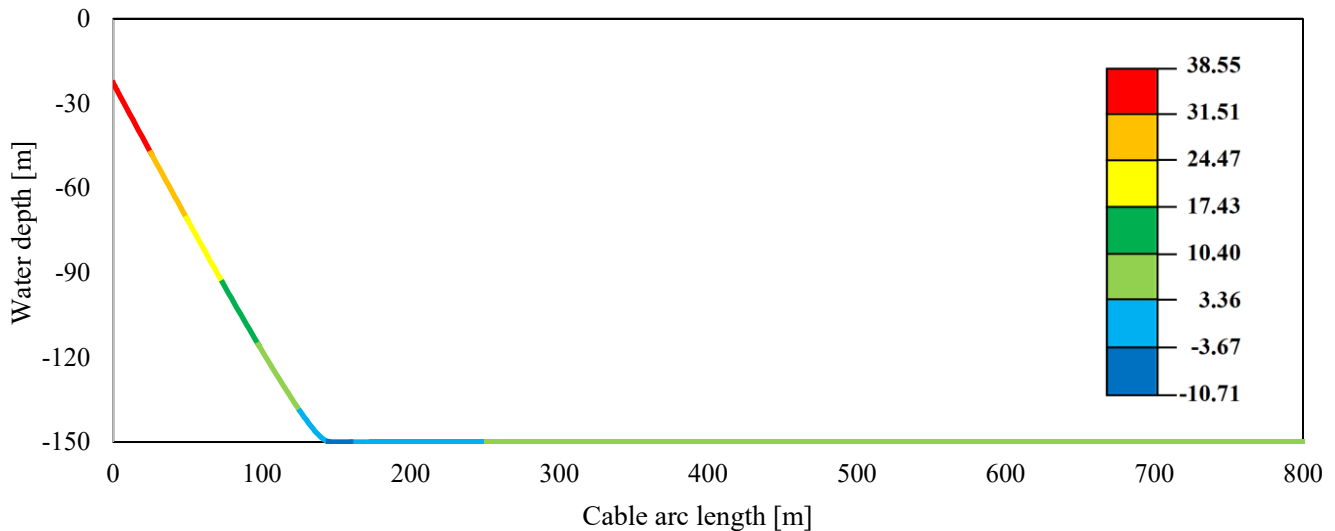


**Figure 19: Minimum tension distribution on configuration profile in C-LC10**

## CONCLUSIONS

This study conducted research on inter-array cabling methods in shallow waters. A substructure with three columns was used to minimize interference between mooring lines and power cables. The power cables are analyzed in four types: catenary, lazy wave, suspended and W-configuration. To simulate a realistic environment, observational data and relevant standards are referenced. The obtained results are as follows.

1. Under ULS conditions, the lazy wave is found to have the best performance among the four shapes. It exhibited 19.00% lower tension compared to the catenary, 25.01% lower compared to the suspended and 26.28% lower compared to the W-configuration, along with 30.52% lower curvature than the catenary, 77.42% lower than the suspended and 60.16% lower than the W-configuration. The selection of the lazy wave is beneficial for ensuring long-term safety.
2. Additionally, the lazy wave shape showed low tension and curvature, with minimal difference in the impact on power cables between the SLS and ULS. Even in rapidly changing environmental conditions, it maintained low tension and curvature, proving superior in terms of shock load as well.
3. When a dynamic power cable has a catenary shape without any means to prevent direct contact with the seabed, it is observed that compressive loads can occur at the touch-down point. Although the values identified in this study are small compared to tensile loads, significant compressive loads may arise due to the cable's configuration deep water depth accompanied by heavy cable weight, and severe environmental conditions, potentially leading to bird caging. Careful consideration during design is necessary to prevent this phenomenon.
4. In this study, an analysis was conducted on four different cabling methods in terms of tension and curvature. However, the results of this study are to be considered preliminary, pending calibration with experimental data. Future research will involve comparative analyses with the free-decay test and regular wave test provided by SINTEF to enhance the reliability of the results.
5. Real ocean environment data obtained from the study will be utilized for fatigue analysis of mooring lines and dynamic power cables. Fatigue Limit State (FLS) will be generated using data observed in the targeted marine area to perform fatigue analysis. Moreover, an essential aspect to be addressed in further research is the cost-effectiveness. A comparative analysis between the installation costs and power production of the four different dynamic power cable configurations will be conducted to determine the payback period and profit based on fatigue life calculations.

## CONTRIBUTION STATEMENT

**Kangho Kim:** Conceptualization; Data Curation; Formal analysis; Investigation; Methodology; Visualization; Writing – Original Draft. **Chunshik Shim:** Funding acquisition; Project administration; Supervision; Resources; Writing - Review & Editing. **Min Suk Kim:** Conceptualization; Supervision; Validation; Writing - Review & Editing. **Daseul Jeong:** Data Curation; Investigation; Writing - Review & Editing.

## ACKNOWLEDGEMENTS

This results was supported by "Regional Innovation Strategy (RIS)" through the National Research Foundation of Korea(NRF) funded by the Ministry of Education(MOE) (Project Management Number of the Foundation: Gwangju Jeonnam Platform 2021RIS-002)

This work was supported korea institute for Advancement of Technology(KIAT) grant funded by the Korea Government(MOTIE) (P0017006 ,The competency Development Program for Industry Specialist)

## REFERENCES

Aker Solutions, (2019). Predictable Offshore Execution – What Does It Take?, Fornebu, Norway.

Ahmad, I. B., Schnepf, A., & Ong, M. C. (2023). An optimisation methodology for suspended inter-array power cable configurations between two floating offshore wind turbines. *Ocean Engineering*, 278, 114406. Retrieved from <https://doi.org/10.1016/j.oceaneng.2023.114406>

American Petroleum Institute (API), 2005. Recommended Practice for Design and Analysis of Stationkeeping Systems for Floating Structures. API Recommend Practice 2SK, 3rd Edition. Washington, D.C.: API. Retrieved from <https://www.api.org/news-policy-and-issues/hurricane-information/gulf-practices>

Chen, W., Guo, S., Li, Y., Gai, Y., & Shen, Y. (2021). Structural configurations and dynamic performances of flexible riser with distributed buoyancy modules based on FEM simulations. *International Journal of Naval Architecture and Ocean Engineering*, 13, 650-658. Retrieved from <https://doi.org/10.1016/j.ijnaoe.2021.07.003>

Det Norske Veritas (DNV), (2016). STANDARD for Loads and site conditions for wind turbines, DNVGL-ST-0437, Oslo: DNV. Retrieved from <https://www.dnv.com/energy/standards-guidelines/dnv-st-0437-loads-and-site-conditions-for-wind-turbines.html>

Det Norske Veritas (DNV), (2019). DNV-RP-C205: Environmental Conditions and Environmental Loads. Oslo: DNV. Retrieved from <https://www.dnv.com/oilgas/download/dnv-rp-c205-environmental-conditions-and-environmental-loads.html>

Hasselmann, K., Barnett, T.P., Bouws, E., Carlson, H., Carwright, D.E., Enke, K., Ewing, J.A., Gienapp, H., Hasselmann, D.E. & Kruseman, P., (1973). Measurements of wind wave growth and swell decay during the Joint North Sea Wave Project (JONSWAP). *Dtsch. Hydrogr. Z.* 1973, 8, 1–95

International Council on Large Electric Systems (CIGRE), (2022). Recommendations for mechanical testing of submarine cables for dynamic applications, Paris: CIGRE. Retrieved from <https://www.e-cigre.org/publications/detail/862-recommendations-for-mechanical-testing-of-submarine-cables-for-dynamic-applications.html>

International Electrotechnical Commission (IEC) (2005). Wind turbines–Part 1: Design requirements, INTERNATIONAL STANDARD IEC 61400-1, London: IEC. Retrieved from <https://webstore.iec.ch/publication/5426>

Korea Hydrographic and Oceanographic Agency (KHOA) (2022). Ocean Data in Grid Framework, Retrieved from <http://www.khoa.go.kr/oceangrid/khoa/koofs.do>

Lavis, J. (2021). Shallow, Mid to Ultra-Deepwater Definitions. *Drillers*. Retrieved from <https://drillers.com/shallow-mid-to-ultra-deepwater-definitions/#comments>

- Li, Y., Guo, S., Guo, Y., Yu, X., Chen, W., & Song, J. (2023). Dynamic responses and robustness performance to moving boundary of double-stepped cable during deep-sea mining. *International Journal of Naval Architecture and Ocean Engineering*, 15(2023), 100546. Retrieved from <https://doi.org/10.1016/j.ijnaoe.2023.100546>
- Lu, Q., Yang, Z., Yang, Y., Yan, J., & Yue, Q. (2017). Study on the Mechanism of Bird-Cage Buckling of Armor Wires Based on Experiment. Proceedings of the ASME 2017 36th International Conference on Ocean Offshore and Arctic Engineering. OMAE2017, June 25-30, Trondheim, Norway. DOI: 10.1115/OMAE2017-61669. Retrieved from <https://doi.org/10.1115/OMAE2017-61669>
- Okpokparoro, S., & Sriramula, S. (2023). Reliability analysis of floating wind turbine dynamic cables under realistic environmental loads. *Ocean Engineering*, 278, 114594. Retrieved from <https://doi.org/10.1016/j.oceaneng.2023.114594>
- Orcina, (2023). Current theory Retrieved from <https://www.orcina.com/webhelp/OrcaFlex/Content/html/Currenttheory.htm>
- Poirette, Y., Guiton, M., Huwart, G., Sinoquet, D., & Leroy, J. M. (2017). An optimization method for the configuration of inter array cables for floating offshore wind farm. Proceedings of the ASME 2017 36th International Conference on Ocean Offshore and Arctic Engineering, OMAE2017, Trondheim, Norway.
- Rentschler, M. U. T., Adam, F., & Chainho, P. (2019). Design optimization of dynamic inter-array cable systems for floating offshore wind turbines. *Renewable and Sustainable Energy Reviews*, 111, 622–635. Retrieved from <https://doi.org/10.1016/j.rser.2019.05.024>
- Rentschler, M. U. T., Adam, F., Chainho, P., Krügel, K., & Vicente, P. C. (2020). Parametric study of dynamic inter-array cable systems for floating offshore wind turbines. *Marine Systems & Ocean Technology*, 15(16-25). Retrieved from <https://doi.org/10.1007/s40868-020-00071-7>
- Schnepf, A., Lopez-Pavon, C., Ong, M. C., Yin, G., & Johnsen, Ø. (2023). Feasibility study on suspended inter-array power cables between two spar-type offshore wind turbines. *Ocean Engineering*, 277, 114215. Retrieved from <https://doi.org/10.1016/j.oceaneng.2023.114215>
- Stiftelsen for industriell og teknisk forskning (SINTEF), (2022). Definition of the INO WIND-MOOR 12MW base case floating wind turbine, Trondheim: SINTEF. Retrieved from <https://hdl.handle.net/11250/2723188>
- Tong, K. C. (1998). Technical and economic aspects of a floating offshore wind farm. *Journal of Wind Engineering and Industrial Aerodynamics*, 74-76, 399-410. Retrieved from [https://doi.org/10.1016/S0167-6105\(98\)00036-1](https://doi.org/10.1016/S0167-6105(98)00036-1)
- W.S. Moon, J.C. Kim, A. Jo & J.N. Won, (2014). Grid optimization for offshore wind farm layout and substation location, in ITEC Asia-Pacific 2014—Conference Proceedings, Beijing. Retrieved from <https://ieeexplore.ieee.org/document/6941124>
- Zhao, S., Cheng, Y., Chen, P., Nie, Y., & Fan, K. (2021). A comparison of two dynamic power cable configurations for a floating offshore wind turbine in shallow water. *AIP Advances*, 11(3), 035302. Retrieved from <https://doi.org/10.1063/5.0039221>